NMR Properties of Formamide: A First Principles and Experimental Study

Juha Vaara,*,† Jaakko Kaski,† Jukka Jokisaari,† and Peter Diehl‡

NMR Research Group, Department of Physical Sciences, University of Oulu, FIN-90571 Oulu, Finland, and Department of Physics, University of Basel, CH-4056 Basel, Switzerland

Received: January 22, 1997; In Final Form: April 23, 1997[⊗]

The tensors corresponding to the second-rank NMR observables, nuclear shielding, quadrupole coupling, and spin−spin coupling of formamide ($HCONH_2$, FA) were determined using several first principles quantum chemical methods. The changes induced on the shielding and quadrupole coupling tensors by intermolecular hydrogen bonding were examined computationally. Liquid crystal NMR experiments were performed for dissolved FA in the SDS and CTAB lyotropic mesophases and their isotropic phases and in the gas phase. We report experimental data on shielding, quadrupole coupling, and spin−spin coupling constants. The convergence of the calculations with the basis set completeness and the treatment of electron correlation were investigated. The calculated and experimental data on the anisotropic properties of the C, N, and O shielding tensors are found to be in good agreement, given the large error limits of the latter caused by the low degree of order of FA in these systems. The medium effects on the observables are found to be readily understood by comparison of structurally relaxed FA monomer and chain trimer calculations. The calculated spin−spin coupling constants are in good agreement with the experimental ones. The anisotropic properties of the corresponding tensors are calculated to be small enough to prevent experimental detection and not to disturb structure determinations by using experimental dipolar couplings. The principal components and the orientation of the principal axis systems of each of the NMR tensors are specified.

1. Introduction

Formamide ($HCONH_2$, FA) is an experimentally and theoretically interesting small molecule for several reasons. It possesses both carbonyl and amide groups and is considered a prototype of the biologically important peptide link.[1] FA is a keen hydrogen bond former; in the neat liquid the molecules are found to chain up through intermolecular N−H···O hydrogen bonds.[2,3] Hydrogen bonding enables FA also to form lyotropic liquid crystalline (LC) systems with surfactant molecules, such as cetyltrimethylammonium bromide (CTAB).[4] The properties of FA have been studied by, for example, microwave and infrared spectroscopic methods and computational chemistry.[5] The monomer geometry and, particularly, whether the molecule is planar have been the main questions. Despite some early confusion, the issue appears to be settled by now in favor of planarity or very near planarity of FA.[6]

In principle, FA is a rich nuclear magnetic resonance (NMR) laboratory in one molecule due to that all its nuclei have magnetic, apart from ^{13}C also quadrupolar (spin ≥ 1) isotopes. Furthermore, all the nuclei are in nonequivalent positions. The ^{14}N nuclear quadrupole coupling constant (χ_N, NQCC) and the asymmetry parameter, η_χ, have been reported in microwave works.[6a,7] Recently, Ludwig et al.[3b] measured the NMR spin−lattice relaxation times in the neat liquid FA for the ^2H, ^{14}N, and ^{17}O nuclei as a function of temperature, enabling estimates of the liquid-state NQCC values to be made. Experimental data on the NMR chemical shifts and spin−spin coupling constants (J_{ij}) have also been reported.[8] Double- and triple-resonance experiments have been used to determine the signs of J_{ij}, except for J_{CN}.[8c,9] The ^1H spectrum of oriented FA in the SDS lyotropic mesophase was explained with a nonplanar geometry in ref 10. However, then it was not ordinary to account for vibrational contributions[11] or solvent-induced anisotropic deformations[12] in the data analysis. Also, the changes of J_{ij} couplings in different surroundings were not considered despite the marked solvent effects reported, e.g., for J_{CN} in ref 8b. In practice, NMR work on FA is complicated by its low solubility in commonly used solvents, except water.[13] Particularly in view of the anisotropic properties of the nuclear shielding ($\boldsymbol{\sigma}_i$), spin−spin coupling ($\mathbf{J}_{ij}$), and quadrupole coupling ($\boldsymbol{\chi}_i$) tensors, the difficulty of dissolving FA in thermotropic LCs makes accurate studies difficult.

Theoretical investigations on the NMR parameters of FA are rather scarce. Calculations of all the shielding tensors,[14] the ^{17}O shielding constant,[15,16] and the ^{13}C shielding tensor[17] at the uncorrelated Hartree−Fock (HF) level have been reported. The NQCC values have also been published recently.[3a,18] Ludwig et al.[3a] performed HF calculations on FA clusters of different types and sizes. They computed the thermal average of the cluster NQCC values and obtained a satisfactory agreement for ^2H, ^{14}N, and ^{17}O nuclei with their relaxation experiments.[3b] The quite modest level of theory (HF/6-31G*) used[3a] is sufficient to account for the main changes occurring in NQCC when comparing an isolated molecule in vacuo with one in the liquid environment. Several solid-state NMR investigations on related compounds have been performed to obtain information on the orientation of the principal axis systems (PAS) of the shielding and electric field gradient tensors.[17,19−21] It was noted in these papers that both hydrogen bonding effects and electron correlation should be taken into account in the modeling. References 15 and 16 contain a discussion of the medium-induced shifts of the ^{17}O shielding constants in molecules containing the C═O group. An excellent treatment of hydrogen bonding effects on the shielding tensor is given in ref 14. Preliminary correlated ^2H and ^{14}N NQCC results of the current research were already given in ref 22. Finally, a well-correlated coupled

* To whom correspondence should be addressed. E-mail Juha.Vaara@oulu.fi; FAX +358-8-5531287.
† University of Oulu.
‡ University of Basel.
⊗ Abstract published in *Advance ACS Abstracts,* June 1, 1997.

S1089-5639(97)00287-9 CCC: $14.00

cluster singles and doubles (CCSD) calculation of the ^{17}O shielding constant was reported in ref 16.

In this work we have investigated the NMR properties of FA using both first principles molecular orbital (MO) calculations and experiments, the latter in the gas phase, in the CTAB and SDS lyotropic LC systems and in the isotropic phases of the latter. We report all the $\boldsymbol{\sigma}_i$, $\mathbf{J}_{ij}$, and $\boldsymbol{\chi}_i$ tensors calculated with the HF method for all applicable nuclei in FA. We performed correlated calculations of $\boldsymbol{\sigma}_i$ and $\boldsymbol{\chi}_i$ using the multiconfiguration Hartree−Fock (MCHF) method. Additionally, many-body perturbation theoretical (MP2 and MP4(SDQ)),[23] coupled cluster doubles (CCD),[24] and quadratic configuration interaction (QCISD)[25] methods were applied for $\boldsymbol{\chi}_i$. Of particular interest is to compare these results to ones from density functional theory (DFT).[26] Complementing the work on $\boldsymbol{\chi}$ presented in ref 22, we now consider results also for the ^{17}O nucleus and include the MCHF, MP*n*, QCISD, and additional DFT methods. $\mathbf{J}_{ij}$ tensors were also calculated using the MCHF method.[27] Finally, to model changes in the NMR properties of FA upon the association of the molecule in the liquid state,[16,28] we calculated the $\boldsymbol{\sigma}_i$ and $\boldsymbol{\chi}_i$ tensors for the central molecule in a geometrically relaxed FA trimer using the HF theory.

We report experimental gas phase J_{HH} and J_{NH} spin−spin coupling constants, $J_{ij} = {}^1/_3$ Tr $\mathbf{J}_{ij}$, and ^{1}H shielding constants $\sigma_H = {}^1/_3$ Tr $\boldsymbol{\sigma}_H$. In the isotropic liquid phase we measured all the chemical shifts, $\delta_i = \sigma_{ref} - \sigma_i$, and the 10 resolvable J_{ij} (those not involving ^{17}O) at various temperatures to determine them at the temperatures corresponding to the LC phase. The orientation tensors of the solute, $S_{\alpha\beta}$, are obtained relatively reliably by applying harmonic vibrational and deformational corrections. The NQCC values are determined, and the anisotropic parts of the ^{13}C, $^{14/15}$N, and ^{17}O shieldings are compared with the theoretical results.

2. Planar Solute in a Uniaxial Liquid Crystal

We review briefly the basics of NMR observables[29] of a solute in a uniaxial LC environment. The general anisotropic NMR spin Hamiltonian is

$$\hat{H} = -1/(2\pi)\sum_i \gamma_i \mathbf{B}_0\cdot(\mathbf{1} - \boldsymbol{\sigma}_i)\cdot\hat{\mathbf{I}}_i + \sum_{i<j}\hat{\mathbf{I}}_i\cdot(\mathbf{D}'_{ij} + \mathbf{J}_{ij})\cdot\hat{\mathbf{I}}_j + \sum_i \hat{\mathbf{I}}_i\cdot\mathbf{B}'_i\cdot\hat{\mathbf{I}}_i \quad (1)$$

where the γ_i and $\hat{\mathbf{I}}_i$ are the gyromagnetic ratio and dimensionless nuclear spin operator, respectively, of the nucleus i. $\mathbf{B}_0 = (0,0,B_0)$ is the magnetic field of the spectrometer (along the laboratory z axis), $\mathbf{D}'_{ij}$ is the direct dipolar coupling tensor of the nuclei i and j, and $\mathbf{B}'_i$ arises from the interaction between the electric quadrupole moment of i with the electric field gradient (EFG) at the nuclear site. Up to the first order in perturbation theory, in the so-called high field approximation, $\hat{H}$ for a molecule in a uniaxial environment becomes

$$\hat{H} = -B_0/(2\pi)\sum_i \gamma_i(1 - \sigma_i^{iso} - \sigma_i^{aniso})\hat{I}_{iz} + \sum_i B_i\hat{I}_{iz}^2 + \sum_{i<j} J_{ij}\hat{\mathbf{I}}_i\cdot\hat{\mathbf{I}}_j + \sum_{i<j}(D_{ij} + {}^1/_2 J_{ij}^{aniso})(3\hat{I}_{iz}\hat{I}_{jz} - \hat{\mathbf{I}}_i\cdot\hat{\mathbf{I}}_j) \quad (2)$$

where the parameters σ_i^{iso} ($=\sigma_i$), σ_i^{aniso}, B_i, J_{ij}, D_{ij}, and J_{ij}^{aniso} determine the structure of a NMR spectrum. The direct dipolar coupling D_{ij} is related to $\mathbf{D}'_{ij}$ by

$$D_{ij} = {}^1/_2 D'^{aniso}_{ij} = -\frac{\mu_0\hbar\gamma_i\gamma_j}{8\pi^2}\left\langle\frac{s_{ij}}{r_{ij}^3}\right\rangle \quad (3)$$

where μ_0 and $\hbar$ have their usual meanings, r_{ij} is the length of the internuclear vector $\mathbf{r}_{ij} = \mathbf{r}_i - \mathbf{r}_j$, and s_{ij} gives the order parameter of $\mathbf{r}_{ij}$ with respect to $\mathbf{B}_0$ (see below). The angular brackets denote rovibrational averaging. The quadrupole coupling is

$$B_i = \frac{3}{2}B'^{aniso}_i = -\frac{3}{4}\frac{eQ_i}{hI_i(2I_i - 1)}F_i^{aniso} \quad (4)$$

where eQ_i is the quadrupole moment of i and the EFG tensor $F^i_{\alpha\beta} = -\partial^2 V_i/\partial\alpha\,\partial\beta$, i.e., the derivative of the electric potential V_i at the site of i. Quantities in the molecule-fixed frame are conveniently expressed in terms of the χ_i tensor, whose largest (in absolute value) principal value is NQCC $= \chi_i = -eQ_iF^i_{cc}/h$. Often $-eq_i$ is used to denote F^i_{cc}.

The anisotropic contributions T^{aniso} of the previous second-rank NMR observables are defined by

$$T^{aniso} = {}^2/_3 P_2(\cos\theta)\sum_{\alpha\beta} T_{\alpha\beta}S^D_{\alpha\beta} \quad (5)$$

where $P_2(x)$ is the second-order Legendre polynomial and θ is the angle between $\mathbf{B}_0$ and the director of the LC phase, $\mathbf{n}$. The Saupe orientation tensor of the molecule is

$$S_{\alpha\beta} = \langle s_{\alpha\beta}\rangle = P_2(\cos\theta)S^D_{\alpha\beta} = {}^1/_2 P_2(\cos\theta)\langle 3\cos\theta_{\alpha,\mathbf{n}}\cos\theta_{\beta,\mathbf{n}} - \delta_{\alpha\beta}\rangle \quad (6)$$

where $\theta_{\alpha,\mathbf{n}}$ is the angle between the Cartesian molecule-fixed axis α and $\mathbf{n}$. The order parameter S_{ij} is the element of $\mathbf{S}$ along $\mathbf{r}_{ij}$. Thus, based on eqs 2 and 3, the Saupe tensor can be determined from the observed anisotropic coupling

$$D_{ij}^{exp} = D_{ij}^{eq} + D_{ij}^{h} + D_{ij}^{ah} + D_{ij}^{d} + {}^1/_2 J_{ij}^{aniso} \quad (7)$$

where D_{ij}^{eq} corresponds to the equilibrium geometry of the molecule. The contributions from the molecular vibrations, D^h and D^{ah} (harmonic[11] and anharmonic,[30] respectively), and deformation,[12b] D^d, should be considered to obtain reliable results. The last term in eq 7 complicates structural information of the dissolved species, which is otherwise available through eq 3. The evaluation of J_{ij}^{aniso} is a demanding task.[31,32] In practice, couplings where J_{ij}^{aniso} is known to be small (HH and CH couplings in general[33]) are used for obtaining $S_{\alpha\beta}$.

The tensor $S_{\alpha\beta}$ is traceless and symmetric, and thus, for a planar FA molecule in the yz-plane (Figure 1), eq 5 can be expanded as

$$T^{aniso} = {}^2/_3[\Delta T_z S_{zz} + {}^1/_2(T_{xx} - T_{yy})(S_{xx} - S_{yy}) + (T_{yz} + T_{zy})S_{yz}] \quad (8)$$

where (x,y,z) are now the molecule-fixed axes and $\Delta T_z = T_{zz} - {}^1/_2(T_{xx} + T_{yy})$ is the anisotropy of $\mathbf{T}$ in that frame. The orientation of the molecule can thus be described using three parameters, S_{zz}, $(S_{xx} - S_{yy})$, and S_{yz}. The combinations of tensor elements appearing in eq 8 can easily be related to the presently calculated properties pertinent to the PAS frame.

3. First Principles Calculations

Quantum chemical methods were applied to obtain the NMR observables of the FA monomer. In each case the wave function (or density) was first optimized, and the properties were

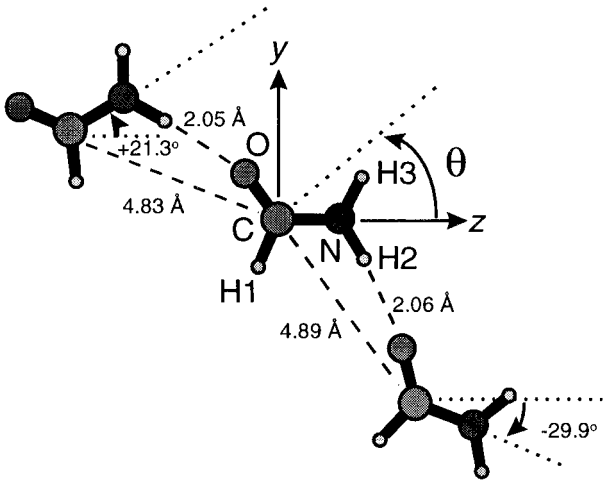

Figure 1. The numbering of atoms and the placement of molecule-fixed coordinate axes in formamide. The data in the text and tables refer to the central molecule. The other two molecules are contained in the trimer calculations, for which some of the intermolecular distances and angles are indicated. θ indicates the sign convention of the in-plane angles corresponding to the directions of the principal axis systems of the shielding, electric field gradient, and spin−spin coupling tensors.

subsequently calculated as expectation values and by perturbation (or response) theory. The trimer was subjected to a full HF geometry optimization with all atoms constrained to remain in one plane, starting from approximately the "fa31" structure reported in ref 3a. The $\boldsymbol{\chi}_i$ and $\boldsymbol{\sigma}_i$ tensors were calculated at the relaxed geometry using the HF theory. The MCHF and partly also the HF results were obtained by using the DALTON software,[34] while Gaussian 94[35] was used otherwise.

The gauge-including atomic orbital (GIAO) method[36] was used for shieldings. GIAO provides with complete gauge-origin independence[37] and rapid basis set convergence[36c,38] as compared with the traditional coupled HF calculations with a common gauge origin.[39] While the HF reference wave function, a single Slater determinant (SD), gives good results in saturated hydrocarbons, multiple bonds and heteroatoms generally demand treatment of electron correlation.[40] GIAO shieldings are available in several program systems. In particular, the HF and MCHF implementations within DALTON and the DFT one in G94 are described in refs 38 and 41, respectively. Theoretical shielding calculations have been reviewed, for example, in ref 42.

Calculation of nuclear EFG is also a common feature in MO programs. Contrary to the other NMR properties, it in principle requires the knowledge of the unperturbed ground-state wave function only.[43] It is, however, generally sensitive to correlation and particularly to the basis set quality.[44−46] To transform the EFG to the $\boldsymbol{\chi}$ tensor, the values $Q = 2.860 \times 10^{-31}$, 20.44×10^{-31}, and -25.58×10^{-31} m^2 [47] for ^{2}H, ^{14}N, and ^{17}O, respectively, were used in this work.

The $\mathbf{J}_{ij}$ are complicated properties as there are several physical mechanisms giving distinct dia- and paramagnetic spin−orbit (DSO and PSO), spin-dipolar (SD), Fermi contact (FC), and the SD/FC cross-term contributions.[33] In DALTON, DSO is calculated as an expectation value over the unperturbed wave function, whereas the other contributions are either singlet[48a] (PSO) or triplet[48b] (SD, FC, SD/FC) response properties.[27] The calculation of properties belonging to the latter category often suffers from the triplet instability problem when using spin-restricted reference wave functions, such as HF. The contributions involving the FC mechanism (FC and SD/FC) converge slowly with improving correlation treatment.[31] Unfortunately, these terms often dominate the spectral parameters. The FC contribution is isotropic and gives nothing to J^{aniso}, while SD/FC does not contribute to J. Reference 49 is a recent review on the calculation of spin−spin couplings.

TABLE 1: Compositions of the Active Molecular Orbital Spaces Used in the MCHF Calculations[a]

wave function	(inactive/RAS1/ RAS2/RAS3)[b]	single/ multiref[c]	% of particles[d]	n_{SD}
RAS-I	(30/00/72/72)	S	66	5 060
RAS-II	(30/00/73/71)	M	66	101 844
RAS-III	(30/00/72/13,6)	S	88	21 716
RAS-IV	(30/00/73/13,5)	M	88	519 456
RAS-V	(30/00/72/21,9)	S	94	54 697

[a] The identifier and the number of Slater determinants, n_{SD}, in the wave function are indicated. [b] Using the nomenclature from ref 52. The maximum number of holes (particles) in RAS1 (RAS3) is two. The occupation of orbitals in RAS2 is unrestricted. The numbers in each category denote the orbitals belonging to A_1 and A_2 symmetry species. [c] Single-reference (multireference) calculation indicated with S (M). [d] The percentage of the total MP2 particle population in the virtual orbitals recovered by the choice of active space.

Planar geometry was adopted in all present calculations, which enabled using C_s symmetry. The r_s microwave geometry of Hirota et al.[6b] was chosen. To model changes due to hydrogen bonding of FA molecules, we also report results for the geometrically relaxed monomer and trimer. The cyclic dimer is energetically the most favorable way of association of two FA molecules.[2b,e,g,50] However, the occurrence of such structures is scarce in liquids,[2c,e,g,3] where more extended chains are preferred.[2a,b,f,51] In our trimer calculations we mimic the linear chain conditions.

Five different restricted active space[52] (RAS) type MCHF wave functions were used for the monomer as described in Table 1. The active spaces have been chosen on the basis of MP2 natural orbital occupation numbers. In each MCHF wave function we keep the 1s core orbitals of the heavy atoms inactive and include the occupied (in the single-determinantal HF picture) MOs and different choices of virtual MOs in the active space. In all cases, 99% of the total MP2 hole population in the occupied MOs is contained in the active space. The three basic choices form a systematic series from minimal to a fairly large virtual active space. They are represented by the single-reference wave functions RAS-I, RAS-III, and RAS-V, where single and double excitations to the virtual MOs are allowed. RAS-II and RAS-IV are multireference functions obtained from RAS-I and RAS-III, respectively, by treating the lowest virtual A_2 symmetry MO (arising from the out-of-plane 2p orbitals of the heavy atoms) on an equal footing with the occupied valence MOs.

We used MP2 and partial fourth-order many-body perturbation theory (omitting the triples contribution), MP4(SDQ). The convergence of these calculations was compared with the results from CCD and QCISD. All MOs were correlated in these calculations.

Three exchange-correlation functionals were used in the DFT calculations: SVWN,[53] which is the common local density approximation, and two electron-density gradient-corrected functionals—BLYP, where the exchange of Becke[54] is combined with the correlation of Lee et al.,[55] and BPW91, where the Becke exchange is used with the correlation by Perdew and Wang.[56]

Common to the requirements placed on the one-particle basis sets by the NMR properties is sufficient flexibility at the regions close to nuclei. The sets used here[57] were HIII and HIV used previously in calculations of $\boldsymbol{\sigma}$,[38,57] $\mathbf{J}$,[58] and $\boldsymbol{\chi}$.[59] For the trimer, the smaller HII basis was supplemented with diffuse s- and p-primitives for C, N, and O and s-primitive for H. The details of these sets, which are originally based on Huzinaga's work,[60]

TABLE 2: Basis Sets Used in the Molecular Orbital Calculations[a]

basis	atom	Gaussian functions: GTO	Gaussian functions: CGTO	contraction pattern	*N*
HII+diff[b]	H	(6s1p)	[4s1p]	{3 2×1 1$^+$/1*}	99
	C, N, O	(10s6p1d)	[6s5p1d]	{5 4×1 1$^+$/2×1 3×1 1$^+$/1*}	
HIII	H	(6s2p)	[4s2p]	{3 3×1/2×1*}	135
	C, N, O	(11s7p2d)	[7s6p2d]	{5 6×1/2 5×1/2×1*}	
HIV	H	(6s3p1d)	[5s3p1d]	{2 4×1/3×1*/1*}	210
	C, N, O	(11s7p3d1f)	[8s7p3d1f]	{4 7×1/7×1/3×1*/1*}	

[a] Identifiers, numbers of primitive and contracted functions, the corresponding contraction patterns, and the number of functions in formamide monomer, *N*, are shown. Spherical Gaussians are used throughout. Polarization functions are denoted by an asterisk and diffuse functions by a superscript plus. [b] The exponents of the diffuse functions were obtained by dividing by three the most diffuse primitive that was already present in the basis for the given type.

TABLE 3: Compositions of the Samples Used and Other Details Related to Experiments[a]

sample	compd	concn (wt %)	remarks
1 (isotropic)	H_2O	84.3	single 5 mm tube; T = 300−340 K; ^{1}H and ^{13}C spectra taken used to determine all the 10 resolvable J_{ij}
	CTAB[b]	11.7	
	^{15}N-FA	3.8	
	H_2SO_4	0.2	
2 (CTAB)	H_2O	62.1	5 mm tube coaxially with a 10 mm tube; T = 297−330 K; $T_{NI} \approx$ 305 K;[c] ^{1}H, ^{13}C, and ^{15}N spectra recorded
	CTAB[b]	35.0	
	^{15}N-FA	2.8	
	H_2SO_4	0.2	
	$^{13}CH_4$	1.5 atm	
3 (CTAB)	H_2O	48.4	5 mm tube coaxially with a 10 mm tube; T = 297−305 K; $T_{NI} \approx$ 301 K;[c] ^{1}H, ^{2}H, ^{13}C, ^{14}N, ^{15}N, and ^{17}O spectra recorded
	D_2O	2.0	
	CTAB[b]	36.8	
	^{15}N-FA	8.0	
	^{14}N-FA	4.3	
	D_3-FA	0.2	
	H_2SO_4	0.2	
	$^{13}CH_4$	1.5 atm	
4 (SDS)	SDS[d]	32.8	approx similar composition of the sample (ignoring isotopomers) as in ref 10; 8 mm tube coaxially with a 10 mm tube; T = 300−350 K; ^{1}H, ^{2}H, ^{13}C, ^{14}N, ^{15}N, and ^{17}O spectra recorded; forms easily several phases and domains
	sodium sulfate	6.4	
	decanol	6.6	
	H_2O	43.8	
	D_2O	0.1	
	^{15}N-FA	8.5	
	^{14}N-FA	3.6	
	H_2SO_4	0.1	
	$^{13}CH_4$	1.0 atm	
5 (gas)	^{15}N-FA	1 mg	spherical 8 mm cell; T = ca. 483 K; ^{1}H spectrum recorded with wide-line probe
	$^{13}CH_4$	1.0 atm	

[a] The chemical shift reference for ^{1}H and ^{13}C was internal ^{13}C-enriched methane in samples 2−5 and external nitromethane (in the annulus of the tube systems) for ^{15}N and ^{17}O in samples 2−4. [b] Cetyltrimethylammonium bromide. [c] Nematic−isotropic phase transition temperature. [d] Sodium decyl sulfate.

are given in Table 2. HIII has been found to be well-converged for calculations of $\boldsymbol{\sigma}_i$ in molecules containing first-row elements, while $\boldsymbol{\chi}_i$ and $\mathbf{J}_{ij}$ generally require better basis sets than shielding. Unfortunately, we had to limit ourselves to HIII with the MCHF work due to disk storage limitations. All the different contributions to $\mathbf{J}_{ij}$ were calculated using HF and RAS-I, whereas the larger MCHF wave functions were used only to calculate the FC and SD/FC terms. RAS-IV turned out to be prohibitively large for calculations of $\mathbf{J}_{ij}$.

In the interest of space we have limited the tabulated material in the Results and Discussion section to cover mostly the best calculations (in terms of the basis sets and correlation treatment used) only. Some of the omitted material can be found in the Supporting Information, and all results are available upon request.

4. Experimental Section

The insolubility of FA in thermotropic LCs EBBA and ZLI 1167 prevented the observation of NMR spectra of FA in the oriented phase of these solvents. The solubility is low probably in all thermotropic LC as they involve similar functional groups, phenyl groups in particular, and FA is known not to be soluble in benzene.[13] It is, however, possible to orient FA in lyotropic LCs which are usually based on water. We used two lyotropic LCs: (I) SDS, which includes sodium *n*-decyl sulfate, sodium sulfate, 1-decanol, and water, and (II) CTAB containing cetyltrimethylammonium bromide and water. Unfortunately, the attainable degree of solute order is lower than that typical in thermotropic systems.

NMR measurements for FA were performed from five samples, in the gas phase and in the isotropic and anisotropic SDS and CTAB systems. The compositions of the samples are shown in Table 3. Samples 2−5 were degassed by vacuum pumping before introducing CH_4 into them. NMR spectra were recorded on the Bruker Avance DSX 300, DPX 400, and DRX 500 spectrometers, using flip angles of either 30° or 90°. Gated ^{1}H decoupling was used with long relaxation delay during ^{2}H acquisition to hinder sample heating.

The J_{ij} were found slightly temperature dependent, especially at temperatures above 320 K. The water mole fraction dependence of J_{CN} in aqueous FA solutions has been reported,[8b] and we observed only a small solvent dependence (at the same

TABLE 4: Nuclear Magnetic Shielding Constants for All Nuclei in Formamide[a]

method	σ_C	σ_N	σ_O	σ_{H1}	σ_{H2}	σ_{H3}
RAS-V/HIII[b]	28.7	167.7	−54.8	23.89	27.24	27.09
HF/HII+diff[c]	−4.4	−7.4	+46.2	−0.12	−2.92	−0.15
HF	33[d]		−81.4[e]			
HF[f]	56.6	200.7	−83.8	23.88	28.62	28.68
CCSD/TZ2P[g]			−54.8			
exp/LC NMR[h]	23.37	151.1	39.06 ± 17.2[i]	22.70	23.40	23.79
exp/LC NMR[j]	24.19	150.9	36.30 ± 17.2[i]	22.74	23.29	23.68
exp/gas phase NMR[k]				22.61	26.24[l]	26.24[l]
exp/liquid NMR		152.5[m]	26.9[n] ± 17.2[i]	22.88[m]	23.38[m]	23.72[m]

[a] Values in ppm. [b] At the experimental r_s geometry. [c] Changes (in ppm) with respect to the monomer (calculated at the same level of theory) are indicated for the central molecule in a relaxed FA trimer. [d] Reference 17. TZ2P basis set. [e] Reference 15. A [3s3p1d]/[2s1p] CGTO basis set for the heavy atoms/hydrogen. [f] Reference 14. A GIAO HF/split-valence calculation. [g] Reference 16. [h] This work. Results for the sample 4 in isotropic phase at 325 K. Chemical shift reference for ^{1}H and ^{13}C was methane, $\sigma_H = 30.61$ ppm and $\sigma_C = 195.1$ ppm,[64] and for ^{15}N and ^{17}O nitromethane, $\sigma_N = -115.59$ ppm[8e,65] and $\sigma_O = -282.1 \pm 17.2$ ppm.[66] [i] Converted to absolute shielding scale by using water, $\sigma_O(H_2O,l) = 307.9 \pm 17.2$ ppm as a reference.[66] [j] This work. Results for the sample 3 at 300 K (σ_N and σ_O) and at 305 K (the rest). [k] This work. Sample 5 at about 483 K. Chemical shift reference as in footnote *h*. [l] Peaks from the separate hydrogens H2 and H3 not resolvable. [m] Reference 8e. Chemical shift reference for ^{1}H was TMS, $\sigma_H = 31.03$ ppm, and NH_3 for N, $\sigma_N = 264.5$ ppm.[65] [n] Reference 8f. At infinite dilution in water at 303 K. A strong dependence on the water mole fraction was observed. For comparison, in the neat liquid at 304 K the result is 4.9 ± 17.2 ppm.

pH level in each sample). This is most likely due to the relative similarity of the samples; the water content varied between 43.8 and 84.3 wt %. In general, the J_{ij} remain practically constant at temperatures near to the phase transitions. (The changes were mostly less than 0.1 Hz.) Thus, we kept the J_{ij} fixed through the analyses of the anisotropic spectra, which were performed using the program Perch[61] with the peak-top-fit or TLS mode.

All the σ_i were temperature and solvent dependent. The σ^{iso} in the anisotropic phase was extrapolated directly from the isotropic phase assuming a continuous linear behavior at temperatures below 330 K; i.e., we assumed that the phase transition has negligible effect. The σ^{aniso} are obtained as differences between the experimental and (extrapolated) isotropic chemical shifts in the LC phase. The σ_H^{aniso} were found to be too small to be determined reliably.

The χ_i were measured from the samples 3 and 4. ^{2}H couplings for ND_2 deuteriums were observable also in sample 4 due to proton exchange with deuterated water. The quadrupole coupling of D1 was detected only in sample 3.

To obtain the gas phase spectrum of FA, a wide-line ^{1}H probe which endures temperatures up to 300 °C was used. From the ^{1}H spectrum at ca. 483 K we could determine two J_{NH} couplings and two ^{1}H shifts, the NH_2 protons being chemically equivalent due to the fast rotation of the group at this temperature. The $^3J_{HH}$ coupling is not detectable at this temperature due to broad lines, and $^2J_{H2H3}$ (between chemically equivalent nuclei) does not affect the spectrum.

The $S_{\alpha\beta}$ for FA in anisotropic phases were determined from the D_{ij}^{exp} couplings obtained from the ^{1}H, ^{13}C, and (in some cases) ^{15}N spectra. Harmonic vibrational (using the theoretical unscaled SCF/4-31G valence force field[62]) and deformational contributions to D_{ij}^{exp} were estimated by the Master program.[63] The contributions from J_{ij}^{aniso} were neglected due to their smallness as seen from the theoretical results. For example, if we use the theoretical values taken from Table 11 (below) with the experimental $S_{\alpha\beta}$, $^1/_2J_{CN}^{aniso}$ becomes 0.02 Hz in sample 4. Simultaneously, the difference between the experimental and fitted *D* couplings in the Master analysis is 0.8 Hz on average.

The structure was fixed to the gas phase r_s geometry,[6b] and four torques acting on the two NH bonds, the CH bond and the CN bond, were left free in the deformational analysis.[12b] The torque acting on the CO bond was fixed to zero because it did not considerably affect the RMS of the fitting process. Allowing this parameter to adjust led also to an unstable behavior of the torques as there was not enough information to determine all of them uniquely. The sensitivity of the results has been checked against the choice of geometry by using an estimated liquid structure, too. The $S_{\alpha\beta}$ of FA in the CTAB system include large relative errors due to the rotation of the NH_2 group and inaccuracies in the J_{ij}, vibrational contributions, and geometry. Together these error sources lead to only qualitative results for T^{aniso}. The situation is much better in the SDS system due to stronger orientation which leads to more reliable results for σ^{aniso} and χ_i. The fact that FA is likely to participate in the formation of the LC phase in the CTAB samples[4b] may also lead to marked changes in the solvent effects in the parameters. In the SDS systems it is known that FA resides in the aqueous regions of the LC phase.[10]

5. Results and Discussion

A. Nuclear Shielding. The experimental and best computed σ_i are given in Table 4. Table 1S (in the Supporting Information) lists the calculated properties for each quantum chemical method used. We have included the data for σ_C from the latter to Table 5 to enable following our discussion. The σ_i^{iso} are measured at temperatures in which the samples are in isotropic phase. The solvent dependence is shown, for example, in σ_C, which is 171.13 and 171.69 ppm with respect to CH_4 in samples 2 and 4, respectively. The strongest temperature effect is seen for σ_O that changes by 0.13 ppm/K in the sample 4. The measured σ_H and σ_C are very accurate due to the internal reference.

When monitored using HF, SVWN, and BPW91 theories, improvements in the basis sets used for the monomer lead to decreasing calculated σ_H, σ_C, and σ_N.[38] For ^{17}O the trend is more complicated. Already the smallest basis, HII+diff, is converged to within a few percent, and entering the HIII level produces a significant change in σ_C only. The changes due to upgrading to the HIV level are small, and the HIII set can be taken to be close to convergence for C and O and fully converged for N and H in FA.

σ_C, σ_N, and σ_O increase substantially with the initial incorporation of electron correlation in the RAS-I calculation. The use of the larger active spaces of RAS-III and RAS-V diminishes the correlation contribution, however, and σ_C, σ_N, and all the σ_H values are reasonably converged in our best calculation, RAS-V. σ_O changes very substantially from RAS-III to RAS-V, but the latter result matches exactly with the CCSD calculation of ref 16. The effects of the use of the multireference wave functions RAS-II and RAS-IV are not systematic for σ_C and σ_N. Multiple excitations decrease σ_O and increase the σ_H

TABLE 5: Example of the Convergence of the First Principles Calculations of Selected NMR Tensors in Formamide[a]

method	σ_C[b]	$\Delta\sigma_C$	η	$F^N{}_{33}$[c]	η	J_{CN}[d]	ΔJ_{CN}	η
HF	18.8	136.9	1.161	0.9377	0.023	17.6	19.0	0.147
RAS-I	32.1	117.9	1.062	0.9157	0.035	15.4	15.7	0.245
RAS-II	36.0	112.2	1.069	0.9218	0.038	15.2	15.6	0.246
RAS-III	28.1	122.6	1.083	0.9015	0.028	13.4	15.5	0.259
RAS-IV	25.9	114.3	1.148	0.9076	0.028			
RAS-V	28.7	121.4	1.130	0.9173	0.026	12.8	15.5	0.253
MP2				0.8255	0.028			
MP4(SDQ)				0.8773	0.027			
CCD				0.8793	0.023			
QCISD				0.8776	0.026			
SVWN	11.3	116.4	1.358	0.7904	0.032			
BLYP	13.4	108.1	1.524	0.8657	0.043			
BPW91	17.4	108.6	1.411	0.8564	0.043			

[a] Shieldings in ppm, EFG in au, and spin−spin couplings in Hz. HIV basis set used except for all RAS-*n* calculations, and the HF calculation of spin−spin couplings where HIII was utilized. The anisotropies and asymmetry parameters in the principal axis systems of the tensors are defined as $\Delta\sigma = \sigma_{33} - {}^1/_2(\sigma_{11} + \sigma_{22})$ and $\eta = (\sigma_{22} - \sigma_{11})/\sigma_{33}$, where the numbering of the axes for each tensor is indicated below. The principal values ordered according to magnitude, (1,2,3), are identified with those ordered according to the symmetry, (*a*,*b*,*c*) (Tables 7, 9, and 11). [b] $\sigma_{11} < \sigma_{22} < \sigma_{33}$, (1,2,3) = (*a*,*b*,*c*). [c] $|F_{11}| < |F_{22}| < |F_{33}|$, (1,2,3) = (*a*,*b*,*c*). [d] $J_{11} < J_{22} < J_{33}$, (1,2,3) = (*b*,*c*,*a*). Only the FC and SD/FC contributions to the tensor were calculated at the indicated level. Other contributions were transported from the RAS-I level.

values markedly, however. We tested also other, small but balanced (in terms of the choice of active MOs based on the MP2 occupation), active spaces with multiple excitations. The convergence of the results was partly quite disappointing, which implies that a single-reference calculation with only up to double excitations and large active spaces can provide qualitatively better results than ones obtained by using smaller multireference active spaces and multiple excitations.[67] The total correlation contributions to σ_C, σ_N, and σ_O are found to be 48, 4, and −30%, respectively, in RAS-V. At the same time, the DFT results have an increasing trend in the SVWN−BLYP−BPW91 order of the functionals. Even the BPW91 results remain significantly below the range of the wave function methods. Apart from σ_C, BPW91 no longer changes the σ_i appreciably as compared to BLYP. The experimental σ_C and σ_N are located between the DFT and RAS-V results.[41] The computed σ_N are relatively closer to experiment than σ_C, and the experimental σ_O is positive, while the calculations produce negative results. The DFT values lie particularly far below those of the wave function methods for σ_O. The discrepancy of the RAS-V calculation and the experimental results can be explained by shifts caused by intermolecular hydrogen bonding,[15,16] as will become evident in the context of the trimer calculations below. RAS-IV produces σ_C and σ_N in fairly good agreement with the experiment. Its poor performance with the hydrogen shielding constants and the fact that its results leave no room for the large hydrogen bonding effects cause us to believe that its success with σ_C and σ_N is accidental.

The difference between the DFT and wave function methods for the shielding constants has already been observed in refs 41, 68, and 69. In particular, the calculations by Cheeseman et al.[41] for a number of molecules using the same functionals as used presently and with a basis set comparable with our HIII set indicates precisely the same disparity as our results do. Apart from the cases with "unusual" bonding conditions (CH_2CCH_2, CO_2, with the italics indicating the difficult nuclei), triple bonds (H*C*N, CH_3CN, N_2), and known examples of pathologically correlated molecules (*NNO*, *CO*), the DFT shielding constants are markedly more negative than either the HF, MP2, or CCSD(T) ones (or experiment).[41,68,69] Among the DFT methods used in ref 41 (excepting the hybrid B3LYP), BPW91 has been found in practically all cases to be the best performing functional, as found also in the present study. The difference between the reported BPW91[41] and MP2[40] results is quite substantial for bonding situations resembling FA. Indeed, in CH_3COCH_3, CH_2O, CH_3NH_2, and CO_2, the observed difference[41] is of similar order of magnitude or larger than the present gap between the present BPW91 and RAS-V results for FA.

As DFT generally provides an improvement over HF for most properties, it is tempting to conclude that the systematic deshielding effect of DFT as compared to the wave function theories is due to the use of so-called uncoupled DFT, i.e., one where the exchange-correlation functional does not contain current dependence.[41,68] Olsson and Cremer[69] and Lee et al.[70] attribute this property to deficiencies in too small DFT orbital energy differences (appearing in the denominator of the expression for the paramagnetic shielding), however, based on the notion that even more deshielded results are obtained by applying current dependent functionals.[70]

The σ_H are generally not sensitive to the correlation treatment.[38] All the calculations reproduce the gas phase experimental fact that H1 is more shielded than the amide group protons (which have very similar σ_H). In the liquid-state experiments of both this work and ref 8e, the difference between H1 and H2/H3 is reduced from that in the gas phase (and vacuum calculations), 4 ppm. Simultaneously, a slight nonequivalence between H2 and H3 appears, presumably due to the preferential intermolecular hydrogen bonding through H2.[2c,g,3b] The MCHF calculations end up roughly 4% and the DFT 2% above the gas phase experimental value; the neglected vibrational corrections in the calculated σ_i may contribute significantly to the discrepancy.

The results of the geometry optimizations of the FA monomer and trimer are given in Table 6. Figure 1 displays the relaxed geometry of the trimer, too. Upon association, the lengths of the CO and NH bonds that are directly involved with the hydrogen bond increase by 0.01 and 0.005 Å, respectively. The CN bond contracts simultaneously by 0.015 Å. These changes correspond roughly to the ones observed when comparing MO and periodic crystal orbital calculations for the monomer and infinite two-dimensional crystal, respectively.[50] The presently calculated hydrogen bond distance, $r_{O\cdots H} = 2.06$ Å, can be compared with Monte Carlo simulations[2c,g] and diffraction experiments[2d] on liquid FA from which 1.85−1.95 Å has been obtained. The slight overestimation in our results would probably be remedied by considering electron correlation in the geometry optimization.[50] The present $r_{N-H\cdots O} = 3.05$ Å matches exactly X-ray diffraction results.[2b,51] A slightly shorter distance of 2.9 Å was, however, obtained by Kálmán et al.[71]

According to Table 4, σ_C and σ_N decrease by 4.4 and 7.4 ppm, respectively, in the trimer as compared to the monomer. The relative change of σ_C is, consequently, larger than in σ_N.

TABLE 6: Theoretical r_e Geometries for Formamide Monomer and Trimer, and the Experimental r_s Geometry for the Monomer[a]

method	r_{CN}	r_{CO}	r_{CH1}	r_{NH2}	r_{NH3}	O−C−H1	H3−N−H2	C−N−H2	O−C−N
HF/HII+diff[b]	1.347	1.188	1.092	0.992	0.995	122.1	119.2	121.3	125.0
microwave exp[b,c]	1.352	1.219	1.098	1.002	1.002	122.5	121.6	120.0	124.7
HF/HII+diff[d]	1.332	1.198	1.090	0.997	0.995	121.6	119.9	120.9	125.3

[a] Bond lengths in angstroms and angles in degrees. [b] Monomer. [c] Reference 6b. [d] Trimer.

TABLE 7: Principal Values σ_{ii} ($i = a, b, c$) and the Orientation of the Nuclear Shielding Tensors of All Nuclei in Formamide[a]

method	property	C	N	O	H1	H2	H3
RAS-V/HIII	σ_{aa}	−73.7	258.8	−179.7	26.19	33.06	34.09
		(−69[b], −53.0[c])	(292.5[c])	(−226.5[c])	(27.4[c])	(36.4[c])	(38.0[c])
	σ_{bb}	50.2	67.8	−330.9	24.63	24.93	23.56
		(53[b], 82.2[c])	(103.7[c])	(−409.4[c])	(22.3[c])	(25.0[c])	(23.3c[g])
	σ_{cc}	109.6	176.5	346.2	20.86	23.74	23.63
		(116[b], 140.7[c])	(206.1[c])	(384.6[c])	(22.0[c])	(24.5[c])	(24.8[c])
	θ_a	42.1 (41[b])	11.7	62.4	59.7	−44.4	45.7
HF/HII+diff[d]	σ_{aa}	+3.9	−11.5	+59.4	+0.16	+1.16	−0.67
	σ_{bb}	−18.8	−16.3	+87.9	+0.35	−4.26	+0.76
	σ_{cc}	+1.9	+5.5	−8.9	−0.86	−5.66	−0.53
	θ_a	+5.1	−1.2	+7.0	−18.9	−10.4	−1.5

[a] The principal axis c is oriented perpendicular to the molecular plane, and the axis a makes the angle θ_a (in degrees, see Figure 1) with the CN bond. The σ_{ii} are in ppm. [b] Reference 17. A GIAO HF/TZ2P calculation. [c] Reference 14. A GIAO HF/split-valence calculation. [d] Relaxed trimer. Changes (in ppm and deg) from the corresponding calculation of the relaxed monomer are indicated.

The changes in σ_{H1} and σ_{H3} are small, but σ_O and σ_{H2} change markedly: the increase (46.2 ppm) in the former is accompanied by a decrease of about 3 ppm in the latter. The change in σ_O agrees excellently with the recent CCSD/DZP result for FA dimer, 43.0 ppm,[16] while that of σ_{H2} corresponds well to the experimental gas-to-liquid shift of σ_{H2}. Generally, these results agree with previous calculations[72] and experiments[8f] on the hydrogen bonding effects on amides, as well as the gas-to-liquid shifts in the carbonyl oxygen.[15] The fact that also σ_{H3} decreases experimentally from gas to liquid implies that H3 may also be involved in intermolecular interactions.[50] According to simulation studies,[2c,e,g] it is almost as probable for a hydrogen bond to be formed through H3 as through the *trans*-hydrogen. As O has two lone pair orbitals, σ_O is prone to even larger changes through hydrogen bonding with two proton donors simultaneously, as found in crystalline FA.[50]

Considering these changes as medium-induced corrections to the RAS-V calculations (corresponding to the in vacuo situation) leads to a very good agreement with the liquid-state experiments, provided that additivity of the effects of multiple simultaneous hydrogen bonds[8f,72a] is allowed. Indeed, when adding the change of 46.2 ppm (multiplied by two due to the two simultaneous H bonds to the O atom) to $\sigma_O = -54.8$ ppm (from the RAS-V calculation), the resulting corrected shielding constant is 37.6 ppm, which is within the range of the experimental results (36−39 ppm). The similar process for nitrogen (there are two H bonds to the amide group) ends up with 152.9 ppm, in good agreement with the experimental 151 ppm. For H2, as apparent from above, the single H bond to this atom brings the calculated value at 24.32 ppm, 1 ppm above the experimental result. It is not obvious how many hydrogen bonds will affect the carbon shielding constant, but at least the two bonds present in our trimer calculation bring the RAS-V result of 28.7 ppm down to 24.3 ppm, close to the experimental results. The approach does not work for σ_{H3}, as there is no H bond to H3 in our example configuration, despite that there is likely to exist one in the liquid state. Hydrogen bonding thus provides with the likely explanation for the majority of the observed discrepancies between the best theoretical and experimental shielding constants and makes us confident with the quality of the RAS-V wave function.

Table 7 shows the principal values σ_{ii} ($i = a, b, c$) and the orientation of the PAS systems from the RAS-V calculation, together with the changes due to hydrogen bonding at the HF/HII+diff level. To give an example, we show the anisotropies $\Delta\sigma$ and asymmetry parameters η in the PAS frame for the $\boldsymbol{\sigma}_C$ tensor calculated with all the present methods in Table 5. The basis set dependence differs slightly from that in σ_i. The heavy atom results are converged at the HIV level, apart from $\eta_{\sigma O}$. The same is not true for H, where changes up to −32% (in $\eta_{\sigma H3}$) are present. The H basis should be made more flexible for accurate description of $\boldsymbol{\sigma}_H$. Electron correlation decreases $\Delta\sigma_C$, $\Delta\sigma_N$, and $\Delta\sigma_O$. The convergence in the series RAS-I−III−V is smooth, but the multireference functions RAS-II and RAS-IV deviate slightly from the general trend. The $\Delta\sigma_H$ are larger and $\eta_{\sigma H}$ smaller in the amide group than for H1. The difference between the density functional and wave function theories is apparent also here: the DFT $\Delta\sigma$ differ by up to 20% from the RAS-V results.

One of the three principal components of all the NMR tensors calculated presently for FA is always directed perpendicular to the molecular plane due to symmetry. For the C and O shielding tensors this is the most shielded component. One of the two in-plane principal axes is oriented roughly along the associated chemical bond for each shielding tensor. For the $\boldsymbol{\sigma}_H$ tensors, this is the most shielded component which makes the angles (note the present sign convention for the angles indicated in Figure 1) −7.5° (H1), +15.6° (H2), and −15.9° (H3) with the corresponding X−H bonds. The least shielded principal component of $\boldsymbol{\sigma}_O$ is at the angle of +27.7° with the C=O bond. The $\boldsymbol{\sigma}_N$ tensor has its most shielded component almost parallel with the CN bond, while the intermediately shielded component of the carbon shielding tensor is along the carbonyl bond. The PAS systems of $\boldsymbol{\sigma}_C$ and $\boldsymbol{\sigma}_O$ are in good agreement with earlier studies of molecules containing the carbonyl group and those of $\boldsymbol{\sigma}_H$ and $\boldsymbol{\sigma}_N$ with ones concerning the amide group.[17,20,21a,72a,73] In particular, we can verify the orientations of all the shielding tensors obtained in the early computational study by Ribas Prado and Giessner-Prettre.[14]

For both C and N in the trimer calculation, the component σ_{bb} that lies roughly in the direction of the FA "chain" decreases by more than 20% as compared to monomer. This is expected on the basis of earlier experimental and theoretical work.[20,72a,74] Similarly, the behavior of the principal components of $\boldsymbol{\sigma}_N$

parallels with what was found for the acetamide dimer.[20] It is interesting to note that a similar reasoning as used for the isotropic shielding constants works for the individual principal values of the carbon shielding tensor: correcting the RAS-V principal components with the trimer−monomer difference brings the calculated values close to the scale of solid-state NMR results for the C═O group in related molecules.[17] As anticipated earlier, both treating electron correlation[17] and intermolecular interactions[17,19,20] thus turns out to be necessary for a quantitative comparison of the calculated and experimental results. For ^{17}O, both the in-plane σ_{ii} components diminish markedly due to hydrogen bonding. For H2, σ_{bb} (roughly perpendicular to the chain) and the out-of-plane σ_{cc} decrease. All these findings concerning the nuclei directly involved in hydrogen bonding are in excellent agreement with earlier calculations for glycylglycine by Chesnut and Phung.[72a] The orientations of $\boldsymbol{\sigma}$ change for C, H1, O, and H2 significantly more than what is expected from the pure geometry change between the monomer and trimer. The shielding tensors appear to "follow" the hydrogen bonding geometry.[72a]

The orientation of FA is very weak in every sample of the present experiments. The problem of solving for the full $\boldsymbol{\sigma}$ tensor is underdetermined when using the data from one sample and temperature. Simultaneous use of the data from several measurements at different temperatures does not improve the situation sufficiently, as the relations between the tensor elements change only slightly. (The underlying group of equations is underdetermined.) However, the experimental and calculated properties can be compared if we determine σ^{aniso} directly from the behavior of the experimental shielding and, for the theoretical σ^{aniso}, use the knowledge of $S_{\alpha\beta}$ (based on the experimental dipolar couplings) and theoretical $\boldsymbol{\sigma}$. The experimental and theoretical (BPW91 and RAS-V) sets of values for σ_i^{aniso} for i = C, N, and O are compared in Figure 2. In the analysis of the D couplings, the J_{ij} values were fixed, which gives the maximum relative errors of approximately 0.3 and 1.8% for SDS and CTAB systems, respectively. (The experimental J_{ij} are given in Table 10.) The relative errors in D_{ij} are bigger in CTAB due to weaker orientation. The spectral analysis using the Perch program provides with average standard deviations of about 1.5 and 0.1% for D_{ij} in SDS and CTAB, respectively.

The sets of D_{ij}^{exp} introduced to the analysis did not allow to iterate the FA geometry. Therefore, the planar r_s structure[6b] was assumed; it was also able to explain all the D_{ij} nearly within the experimental errors. If we consider solvent-induced changes in the geometry (deduced based on refs 6b, 50, and 71 along with the presently calculated changes from the monomer to the trimer) and recalculate the orientation tensors, we obtain a measure of the sensitivity of the results to the choice of geometry. For example, for σ_C^{aniso} in the SDS system, the change is 4%. The final relative error limits are obtained by considering the other sources of error, too. The uncertainties of approximately 0.3 and 1.5% in the experimental J_{ij} and D_{ij}, respectively, were found in test Master runs to result in far smaller errors in $S_{\alpha\beta}$ as compared to those originating from the choice of geometry, however.

For σ_C^{aniso} and σ_O^{aniso}, the calculated and experimental data seem to agree well, considering the magnitude of the present error limits. For the same reason, the differences between the present monomer and trimer calculations are irrelevant for the comparison.

B. Quadrupole Coupling. The experimental and best computed quadrupole coupling data are collected in Table 8. A full set of calculated results is available in Table 2S (in the Supporting Information). To give an example, Table 5 lists $F^{\text{N}}{}_{cc}$ and $\eta_{\chi\text{N}}$ for all methods. Improvements in the basis are accompanied by a decrease in the calculated χ. HIV is not fully converged for χ_N. Similarly, the χ_D show changes of the order of 5% from HIII to HIV. The conclusion is, therefore, that the HIV set should be made more flexible for the N and hydrogen atoms (and very likely for O, too). ^{2}H is elaborated more fully for methyl halides in ref 45, from which it may be estimated that the HIV set exaggerates the χ_D by approximately 4%.

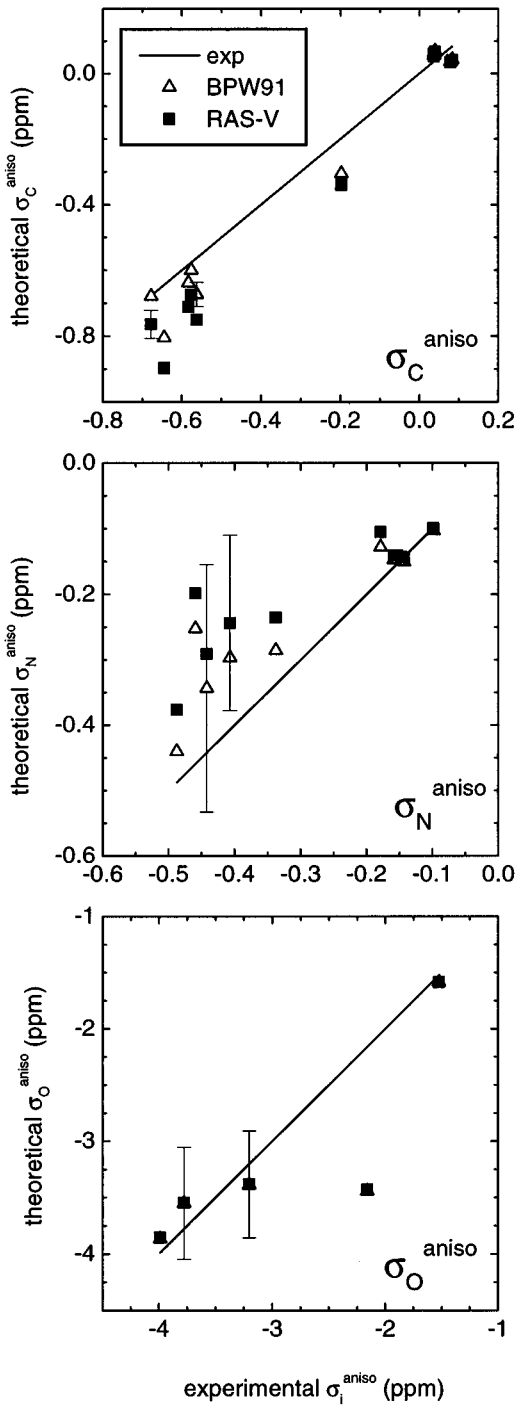

Figure 2. Comparison of the anisotropic nuclear shieldings in formamide as determined experimentally from the observed chemical shifts, and theoretically by the RAS-V and BPW91 calculations for the monomer. (a) Carbon (samples 2−4), (b) nitrogen (samples 2−4), and (c) oxygen (sample 4). Error bars are drawn to some of the calculated points to illustrate the effect of the inaccuracy of the orientation tensor.

Electron correlation decreases χ_N and χ_O, while it hardly affects the χ_D. Comparison of the MCHF calculations shows

TABLE 8: Nuclear Quadrupole Coupling Constants, χ_i, and Asymmetry Parameters, η_χ, for the ^{2}H, ^{14}N, and ^{17}O Nuclei in Formamide[a]

method	χ_N	η_χ	χ_O	η_χ	χ_{D1}	η_χ	χ_{D2}	η_χ	χ_{D3}	η_χ
QCISD/HIV	−4215	0.026	9596	0.058	183.5	0.052	284.0	0.184	282.4	0.160
HF/HII+diff[b]	+605	+0.176	−440	−0.050	+1.3	−0.008	−30.9	+0.006	+0.5	−0.013
MP2/TZVp[c]	−4207	0.031	9166	0.103	191.5	0.059	291.0	0.191	286.3	0.175
HF/6-31G*[d]	−4613	0.028	10210	0.035	181.9	0.036	291.9	0.188	286.6	0.173
cluster model[d]	−3495	0.394	9209	0.402	182.0	0.038	221.0	0.223	285.0	0.147
microwave[e]	−3848	0.019								
microwave[f]	−3852	0.028								
NMR T_1[g]	−2840		9180		170.0		233.0		280.0	
LC NMR[h]	−2700 ± 200		6400 ± 900				240 ± 20		250 ± 30	
LC NMR[i]	−2700 ± 200		6800 ± 900				270 ± 20		280 ± 30	
LC NMR[j]	−2600 ± 800		11300 ± 400		70 ± 4		200 ± 14		400 ± 60	
LC NMR[k]	−3200 ± 800		11000 ± 400		72 ± 4		190 ± 14		340 ± 60	

[a] χ_i in kHz. Present calculations use the definition $\eta = (F_{22} - F_{11})/F_{33}$, where $|F_{11}| < |F_{22}| < |F_{33}|$. [b] Changes (in kHz for the χ_i) with respect to the monomer (calculated at the same level of theory) are indicated for the central molecule in a relaxed FA trimer. [c] Reference 18. [d] Reference 3a. The results have been scaled using the most accurate known Q_i (see text), unlike in the original reference. [e] Reference 7b. [f] Reference 6a. [g] Reference 3b. Measured in the neat liquid. Assumed zero η. χ_{D1}, χ_{D2}, and χ_O were found T dependent. [h] This work, assuming zero η. Results for sample 4 as average of several measurements. [i] As in footnote *h*, but the experimental χ has been corrected for the neglected η. The orientation of the EFG PAS with respect to the (x,y,z) frame and η_χ have been taken from the theoretical calculations. [j] As in footnote *h* but for sample 3. [k] As in footnote *j* but corrections were applied as in footnote *i*.

that the NQCCs have converged apart from χ_O where a 3.5% increase is noted from RAS-III to RAS-V. The η values change substantially more than the NQCCs between different calculations.[45] Multireference functions have only a very little effect on the NQCC values. Progression along the perturbation series HF−MP2−MP4(SDQ)−CCD−QCISD is reflected in χ_N and χ_O. While MP2 overshoots the correlation-caused decrease in the $|\chi_i|$ (changes from the HF level −12%), MP4(SDQ) gives a correction to the opposite direction. QCISD results are closer to MP4(SDQ) than CCD, implying that the single substitutions are important for these properties.

The DFT calculations SVWN, BLYP, and BPW91 form a series that appears also to be converging, although formally there is no need for this to happen. First, comparing SVWN with HF, both $|\chi_N|$ and χ_O decrease by over 10% in SVWN, and the ^{2}H parameters are unaffected. Introducing gradient corrections in BLYP gives a large opposite change in $|\chi_N|$ and a smaller change in χ_O. Contrary to the many-body perturbation series, the χ_D are also affected, as they decrease by 2−3% in BLYP as compared to SVWN. The change of the correlation functional to BPW91 then gives a smaller opposite correction, with the change in all the χ of the order of 1%.

Comparing with the gas phase experiments[6a,7b] for ^{14}N, the computed HF and MCHF values are well over 10% above the experiment. Also, the MP*n*/CCD/QCISD series converges to some 10% above the experiment, with the MP2 value being fortuitously quite close. The calculated values correspond to a rigid molecule, which may be a dubious approximation as the amide group has low-energy vibrational modes associated with it. The main reason for the discrepancy is, however, that the same basis sets were used for the calculation of the $\boldsymbol{\chi}$ as for the other NMR properties; particularly, HIII used with MCHF is rather modest. This is apparent from the success of locally large sets in refs 44 and 45.

For χ_O and χ_D there are no experimental gas phase data available, and we can make a qualitative comparison with the QCISD/HIV calculation, which can safely be considered the best current one. The upward deviation of χ_O from the real value may be as large as 10% in QCISD/HIV (judging from the basis set incompleteness and the ^{14}N results). For ^{17}O, RAS-V deviates upward by 4% from QCISD/HIV, whereas BPW91 lies 3% below this reference. For ^{2}H, the overestimation of QCISD/HIV is likely to be about 4% (from the basis set error[45]). RAS-V lies somewhat (3.8% for D1, 1.5% for the amide group D nuclei) above QCISD/HIV. A RAS-V/HIV calculation would probably give results agreeing well with our reference calculation. The "DFT limit" (BPW91/HIV) for the χ_D values is slightly (around 1%) below QCISD. As with the shielding constants, DFT appears to converge to a limiting value different from that obtained from the wave function methods. The difference is smaller for χ, however.

TABLE 9: Principal Values F_{ii} ($i = a, b, c$) and the Orientation of the Electric Field Gradient Tensors of the Quadrupolar Nuclei in Formamide[a]

method	property	N	O	D1	D2	D3
QCISD/HIV	F_{aa}	−0.4273	1.5965	−0.2731	−0.4227	−0.4202
	F_{bb}	−0.4503	−0.7516	0.1295	0.1725	0.1765
	F_{cc}	0.8776	−0.8449	0.1437	0.2501	0.2437
	θ_a	33.2	34.9	67.1	−59.9	60.8
HF/HII+diff[b]	F_{aa}	−0.033	−0.073	−0.002	+0.046	−0.001
	F_{bb}	+0.159	−0.141	+0.002	−0.020	+0.003
	F_{cc}	−0.126	+0.214	+0.000	−0.026	−0.002
	θ_a	−45.8	+0.7	−0.5	+0.1	+0.4

[a] Axes as in Table 7. The F_{ii} are in au. To change the values into quadrupole coupling tensor elements in kHz, the following scaling factors should be used: ^{14}N, −4803; ^{17}O, 6010; and ^{2}H, −672 kHz/au. [b] Relaxed trimer. Changes (in au and deg) from corresponding calculation of the relaxed monomer are indicated.

Table 9 contains the relevant tensorial properties of EFG, expressed in the PAS frame. The main (largest in absolute value) principal components of the $\boldsymbol{\chi}_O$ and $\boldsymbol{\chi}_D$ tensors lie in the molecular plane, while that of $\boldsymbol{\chi}_N$ is the out-of-plane component. These findings appear to be generally valid for the amide nitrogen and hydrogen nuclei.[19,21] The bond system defines the direction of the principal axes: The largest component of the EFG tensor is very precisely (within 1°) along the associated bond for the deuterium nuclei, as usual,[21,75] and perpendicular to the C═O bond for oxygen. The orientation of the two in-plane axes of $\boldsymbol{\chi}_N$ is less obvious; it even shows a sensitivity to the method of computation.[22] However, the range of positive angles θ_a obtained from the various methods used presently coincides with the solid-state NMR results by Eichele et al.[19]

The present experimental situation is nearly the same for $\boldsymbol{\chi}$ as for $\boldsymbol{\sigma}$. The same $S_{\alpha\beta}$ are used and the error limits are extracted similarly. Due to inaccuracies and similar $S_{\alpha\beta}$ in different measurements, it is not possible to determine the full $\boldsymbol{\chi}$ tensors. However, χ_i can be derived from the experimental data provided that the orientation of F^i_{cc} with respect to the external magnetic field is known. χ_i is obtained by transformation of the $S_{\alpha\beta}$ tensor in the molecular frame (derived from the D_{ij}^{exp}) to the PAS of

the EFG. Equation 4 reduces then to the form

$$B_i = \frac{3}{4}\frac{\chi_i}{I_i(2I_i-1)} S^D{}_{cc} P_2(\cos\theta)\left[1+\frac{\eta_\chi}{3}\frac{S^D{}_{aa}-S^D{}_{bb}}{S^D{}_{cc}}\right] \quad (9)$$

The significance of the term containing η_χ in the square brackets is determined by the orientation tensor in the PAS. Table 8 displays both purely experimental χ_i, where the $\eta_\chi = 0$ assumption has been made, and ones where the theoretical *orientation* of the EFG PAS and η_χ (originating from the present calculations) in that frame have been used for corrected χ_i.

The LC NMR and previous T_1 relaxation experiments[3b] reveal that changes take place in the NQCCs on entering the liquid phase. $|\chi_N|$ is reduced by roughly 1 MHz from the gas phase experiments.[6a,7b] Comparing the relaxation experiment with our QCISD/HIV calculation, χ_{D1} decreases by about 7% and χ_{D2} by 18% in the neat liquid FA. The trimer calculations reproduce the decrease in $|\chi_N|$; it is reduced by 605 kHz from the monomer. Our results parallel qualitatively those of related calculations of the acetamide−formaldehyde complex, where a corresponding decrease in $|\chi_N|$ and a large increase in the associated asymmetry parameter were observed.[19] If both D2 and D3 participate in hydrogen bonding, we would expect roughly twice the decrease, which brings the QCISD result down to 3005 kHz, in fair agreement with the experimental 2840 kHz. A similar treatment causes χ_O to decrease to 8716 kHz, which is below the experimental 9180 kHz. However, test calculations of the trimer with the HF geometry but at the BPW91 level of theory (not shown) resulted in a far smaller decrease (116 kHz) of χ_O due to hydrogen bonding. No such sensitivity to the method used was observed for any other electric field gradients (nor shieldings).

There is a disagreement between the experimental relaxation[3b] and the two present sets of LC NMR data for χ_O and the χ_D values in Table 8. This is probably partly due to the different environments: neat liquid and different LC systems where FA is in different physical environments, as noted above. The error limits are also quite sizable in both experiments. The weak orientation achieved in the lyotropic LC solutions adds to the experimental uncertainty significantly: the analysis may result in relatively small error bars and apparently precise results. Particularly the χ_{D1} is not very reliable as it was obtained from the CTAB system.

Contrary to the experiments, we obtained a slight increase in χ_{D1} in the trimer calculation. χ_{D2} decreases in the trimer by 10% as compared to the monomer. In this case, the "H-bond"-corrected QCISD result is 253.1 kHz, i.e., well within the range of experimental results. Table 9 reveals that the out-of-plane F_{cc} decreases for N, O, and D2 in the trimer. Simultaneously, the in-plane components decrease for D2, and the components $F^N{}_{bb}$ and $F^O{}_{bb}$ along the chain decrease and increase, respectively. The orientation of the PAS of $F^N{}_{\alpha\beta}$ turns by 45°. The orientation of the PAS of the oxygen and deuterium quadrupole coupling tensors does not reflect hydrogen bonding geometry to the extent observed for the shielding tensors. Instead, the tensors remain fixed to the nuclear framework to a good accuracy.

Generally, our trimer calculations appear to give a semiquantitatively correct description for the main changes in the NMR parameters (nuclear shielding and quadrupole coupling) from gas to liquid. However, we have completely neglected dynamics and, for example, the possibility of multiple simultaneous hydrogen bonds through both the amide group, and the oxygen atom is treated based on a simple additivity argument. Thus, the results cannot be expected to reproduce the changes fully quantitatively.

C. Spin−Spin Coupling. The calculated and experimental J_{ij} are given in Table 10. Table 3S (Supporting Information) contains the results of all the present calculations. The data for $\mathbf{J}_{CN}$ are presented in Table 5, too. All the calculations of the 15 different $\mathbf{J}_{ij}$ were performed with HIII basis. Thus, no information about the convergence with respect to the basis set is available from the present study. From experience gained in other computational studies,[32,58] HIII should be nearly converged.

The progression from the HF method up to RAS-V reveals that HF does reasonably well for this molecule, contrary to expectations. The signs of the J_{ij} given by HF are correct (same as in RAS-V), except for the small $^3J_{OH2}$. Even the magnitudes are reasonably well described for most couplings. Comparison of the MCHF results RAS-I to RAS-V displays changes mostly of the order of 15% and below on entering the next level. In particular, the changes associated with the last step from RAS-III to RAS-V are 8% and smaller, apart from $^2J_{H2H3}$ where the residual change is 11.4%. This indicates excellent overall convergence, as the difference between the active spaces of the two calculations is substantial.

Experimental liquid phase results from the present work are available for all the J_{ij} not involving ^{17}O. The calculated HH and NH couplings are in good agreement with the present values and those reported earlier.[8e] The MCHF calculations correctly reproduce the signs and orders of magnitude of all the 10 known J_{ij}. In our best calculation, RAS-V, the large couplings are calculated correctly typically to within 10%. The relative deviation of the small couplings $^2J_{H2H3}$ and $^3J_{H1H2}$ from the experiment is larger, although acceptable when considered in hertz.

Table 10 displays also the contributions of the different physical mechanisms to the calculated J_{ij}. The FC contribution is the dominant (responsible for 70% or more) one in most of the RAS-V couplings; the only exceptions are $^3J_{OH3}$ (−4%) and $^1J_{CO}$ (50%). This being stated, limiting the calculations for FC only would produce misleading results in all cases involving ^{17}O and the $^2J_{CH}$ couplings. In $^3J_{H1H3}$ and $^2J_{H2H3}$, as often in HH couplings, the large DSO and PSO cancel almost exactly, and the simultaneous small magnitude of the SD term allows FC to appear as the sole effective mechanism. FC is truly the only significant factor in $^1J_{CH1}$, $^1J_{NH2}$, $^1J_{NH3}$, and $^2J_{NH1}$. Looking at the convergence of the FC term with the level of calculation (in Table 4S in the Supporting Information), RAS-V appears to be fairly saturated in most of the couplings. Of the remaining, less converged ones, $^2J_{CH3}$ is small but qualitatively well described when compared with the experimental number. Generally, doubts remain only for $^3J_{OH3}$ and $^1J_{CO}$.

DSO gives usually a small contribution to J_{ij} when at least one of the nuclei involved is not H. The exceptions to this are the $^2J_{CH}$ couplings and $^3J_{OH2}$, where DSO and PSO add up with similar signs to give significant total orbital contribution. PSO is, additionally, effective in $^2J_{OH1}$ and $^1J_{CN}$. SD is the most time-consuming part of the calculation of the $\mathbf{J}_{ij}$, and it often gives only a small contribution to J_{ij}. This is also found to be the case for FA, apart from $^3J_{H1H2}$ and some of the couplings to ^{17}O. Fully negligible changes are caused to the DSO contribution by the introduction of the modest correlation treatment in RAS-I. The changes in PSO in all the ^{17}O-involving couplings are large enough to render their estimates not very reliable.

In Table 11 the principal values and the orientation of PAS of the $\mathbf{J}_{ij}$ are given. In all the one-bond couplings and in $^2J_{CH2}$ and $^2J_{CH3}$, one of the two in-plane axes is nearly parallel with the internuclear vector. The data indicate that the tensorial

TABLE 10: Spin−Spin Coupling Constants in Formamide[a]

method	mechanism	$^2J_{H2H3}$	$^3J_{H1H2}$	$^3J_{H1H3}$	$^1J_{CH1}$	$^2J_{CH2}$	$^2J_{CH3}$	$^1J_{NH2}$	$^1J_{NH3}$	$^2J_{NH1}$	$^2J_{OH1}$	$^3J_{OH2}$	$^3J_{OH3}$	$^1J_{CN}$	$^1J_{CO}$	$^2J_{ON}$
RAS-V[b]	DSO	−6.5	−0.5	−4.2	1.0	−0.7	−0.7	0.2	0.2	−0.1	0.4	0.5	0.1	0.1	−0.1	0.0
	PSO	7.3	0.2	4.1	−0.9	−0.5	−0.5	1.5	1.3	−0.2	1.2	0.7	1.3	−2.2	12.9	1.6
	SD	−0.1	0.1	0.0	−0.1	−0.1	−0.2	0.1	0.1	0.0	0.0	0.1	0.3	0.0	−1.6	−0.5
	FC	3.1	0.9	12.0	183.1	4.0	−2.9	64.4	64.2	11.9	−7.8	−2.3	−0.1	15.0	9.5	−2.4
	total	3.8	0.8	11.8	183.2	2.8	−4.2	66.2	65.8	11.6	−6.2	−1.0	1.7	12.8	20.7	−1.3
exp/liquid[c]		2.18	2.25	13.90	193.11	2.68	−3.69	65.24	63.23	9.62				10.57		
exp/gas phase[d]								58.3	58.3	15.3						
exp/liquid		2.3−2.6[e−h]	2.1−2.3[e−h]	12.9−13.9[e−h]	183.6−192.8[f,i]	2.9[f]	−5.2[f]	64.4−65.6[e,g,h,j]	62.0−62.6[e,g,h,j]	10.2−13.5[e,g,h,j]				13.9−14.8[k]		

[a] The couplings are in Hz. Couplings to nitrogen always refer to the ^{14}N isotope and those to hydrogen to the ^{1}H isotope. The present calculations were performed using the basis set HIII. [b] The contributions from the different physical mechanisms are indicated. Only the FC contribution was calculated at the RAS-V level. Other contributions were transported from the RAS-I calculation. [c] This work. The isotropic sample 1 was used. [d] This work. See footnote *l* in Table 4. [e] Reference 8e. [f] Reference 8c. [g] Reference 8a. [h] Reference 9. [i] Reference 8d. [j] Couplings reported for ^{15}N changed to ^{14}N by multiplying with the ratio $\gamma_{14N}/\gamma_{15N} = -0.713\,053$. [k] Reference 8b. The result was found to depend on the water mole fraction in the aqueous solution of FA.

TABLE 11: Calculated Principal Values $J_{\alpha\alpha}$ ($\alpha = a, b, c$) and Orientation of the Principal Axis System of the Spin−Spin Coupling Tensors in Formamide[a]

	J_{aa}	J_{bb}	J_{cc}	θ_a
$^2\mathbf{J}_{H2H3}$	11.2	11.9	−11.8	39.1
$^3\mathbf{J}_{H1H2}$	2.4	0.7	−0.8	−9.2
$^3\mathbf{J}_{H1H3}$	14.2	10.6	10.5	12.6
$^1\mathbf{J}_{CH1}$	161.5	192.9	195.2	67.0
$^2\mathbf{J}_{CH2}$	2.0	6.0	0.4	−32.8
$^2\mathbf{J}_{CH3}$	−4.1	−2.2	−6.3	33.5
$^1\mathbf{J}_{NH2}$	53.3	73.8	71.6	−60.4
$^1\mathbf{J}_{NH3}$	53.2	73.2	71.0	63.4
$^2\mathbf{J}_{NH1}$	12.4	11.4	11.1	−44.5
$^2\mathbf{J}_{OH1}$	−4.3	−11.8	−2.6	−22.4
$^3\mathbf{J}_{OH2}$	−4.9	0.6	1.3	−1.8
$^3\mathbf{J}_{OH3}$	1.7	0.7	2.6	29.4
$^1\mathbf{J}_{CN}$	23.1	4.7	10.6	3.7
$^1\mathbf{J}_{CO}$	−17.3	64.2	15.3	−55.9
$^2\mathbf{J}_{ON}$	−4.9	4.6	−3.6	10.5

[a] $J_{\alpha\alpha}$ in hertz. The FC and SD/FC contributions are taken from the RAS-V calculation, while the others are from RAS-I. The principal axis *c* is oriented perpendicular to the molecular plane, and the axis *a* makes the polar angle θ_a (in degrees, see Figure 1) with the CN bond.

character of all the couplings is quite negligible. The importance of J_{ij}^{aniso} must be weighed against the magnitude of the corresponding D_{ij} and J_{ij} (see eq 2). Indeed, in a typical SDS measurement, the relative contribution of J_{ij}^{aniso} in $2D_{ij} + J_{ij} + J_{ij}^{\text{aniso}}$ is below 0.05% in all cases but for the CN coupling, where it is 0.2%. Thus, the anisotropic contributions to all $\mathbf{J}_{ij}$ in FA are hardly experimentally detectable due to the low orientation achieved in the applicable solvents.

There is no clear pattern in the importance of the different physical contributions to the J_{ij}^{aniso}. DSO and PSO largely cancel in the J_{HH} and J_{CH}, which often makes the SD/FC term the most important contribution. Notably, in the J_{OH} couplings there is large cancellation arising from sizable terms with different signs.

6. Conclusions

We have used various quantum chemical methods to calculate the six nuclear shielding, five quadrupole coupling, and 15 spin−spin coupling tensors in formamide. The effects on the shielding and quadrupolar tensors caused by the association of the FA molecules in the liquid state were estimated by comparison of calculations performed on structurally relaxed monomer and a chain-conformation trimer. We have also measured NMR spectra of FA in various surroundings: in the gas phase, in both SDS and CTAB liquid crystalline states, and in the isotropic liquid state of these materials.

The convergence with the one-particle basis set size has been monitored in the calculations. The quadrupole coupling tensors are found to be more demanding than the shielding tensors in this respect. The effects of electron correlation have been investigated and found significant for the shielding and quadrupolar tensors of the heavy atoms in FA, contrary to the hydrogens. The best density functional and wave function results bracket the experimental σ_C and σ_N, contrary to σ_O which is affected by hydrogen bonding in solution. The main effects induced by the liquid environment on the shielding constants are well understood based on the trimer calculations. Our results fit into the established pattern that DFT results in systematically, and in some cases significantly, too negative shielding constants. A multiconfiguration Hartree−Fock calculation with a large active space (RAS-V) turns out to be the best method applied in the present paper. The results for the anisotropic parts of the heavy atom shielding tensors are qualitatively corroborated

by the LC NMR experiments. Completely independent experimental information on the individual shielding tensor elements is inaccessible due to the generally low degree of order achievable for FA in lyotropic solutions. The orientation of the principal axis systems of the shielding tensors is seen to be roughly determined by the framework of chemical bonds of the molecule. The results are in excellent agreement with earlier studies of related molecules.

The present calculations converge to values exceeding in magnitude the gas phase experimental value of the ^{14}N quadrupole coupling constant. This is mainly due to the use of the same basis sets that give converged results for the other NMR quantities instead of locally dense ones. The different wave function approaches and DFT give slightly diverging results for χ_O, while the mutual agreement is good for the χ_D. The liquid environment induces changes to the χ_N and χ_D that can be reasonably rationalized, again, by the trimer calculations. The present LC NMR results for χ_N and the amide group deuteriums agree well with those based on relaxation studies. χ_O shows large changes between various surroundings, but large experimental error limits prevent definite conclusions in this case. The principal axis directions of the electric field gradient tensors are strictly fixed to the bond system.

The calculated spin−spin coupling constants are in good agreement with the 10 couplings that are also available from the present and previous experiments. The contributions of the different physical mechanisms to the isotropic part of the tensors are indicated. The tensor elements responsible for J_{ij}^{aniso} were theoretically found to be too small for experimental detection in the present LC systems. Their smallness makes it likely that they contribute negligibly to the observed dipolar couplings also in NMR structure determinations of systems containing FA, the peptide link, or related structures. For all the one-bond couplings, one of the two in-plane principal axes is always directed along the vector connecting the coupled nuclei.

Acknowledgment. We thank the Academy of Finland and Neste Oy Foundation for financial support. J.V. expresses his gratitude also to the Vilho, Yrjö, and Kalle Väisälä Fund and J.K. to the Alfred Kordelin Fund. Both J.V. and J.K. thank Dr. Juhani Lounila for many discussions regarding liquid crystal NMR. Kenneth Ruud (University of Oslo, Norway), is thanked for access to the DALTON program and Dr. Michał Jaszuński for providing information on his results prior to publication (ref 16). The Center for Scientific Computing (Espoo, Finland) provided the computational facilities. The unknown referees are thanked for helpful suggestions.

Supporting Information Available: Tables 1S, 2S, and 3S containing the results of the full series of calculations for the nuclear shielding constants, quadrupole coupling constants, and spin−spin coupling constants in FA and Table 4S containing the convergence of the calculated Fermi contact contribution to the spin−spin coupling constants (4 pages). Ordering information is given on any current masthead page.

References and Notes

(1) Stryer, L. *Biochemistry*, 3rd ed.; Freeman: New York, 1988.

(2) (a) Siegbahn, H.; Asplund, L.; Kelfve, P.; Hamrin, K.; Karlsson, L.; Siegbahn, K. *J. Electron Spectrosc. Relat. Phenom.* **1974**, *5*, 1059. (b) Ohtaki, H.; Funaki, A.; Rode, B. M.; Reibnegger, G. J. *Bull. Chem. Soc. Jpn.* **1983**, *56*, 2116. (c) Jorgensen, W. L.; Swenson, C. J. *J. Am. Chem. Soc.* **1985**, *107*, 569. (d) Wiesmann, F.-J.; Zeidler, M. D.; Bertagnolli, H.; Chieux, P. *Mol. Phys.* **1986**, *57*, 275. (e) Sagarik, K. P.; Ahlrichs, R. *J. Chem. Phys.* **1987**, *86*, 5117. (f) Østergård, N.; Christiansen, P. L.; Nielsen, O. F. *J. Mol. Struct. (THEOCHEM)* **1991**, *235*, 423. (g) Gao, J.; Pavelites, J. J.; Habibollazadeh, D. *J. Phys. Chem.* **1996**, *100*, 2689.

(3) (a) Ludwig, R.; Weinhold, F.; Farrar, T. C. *J. Chem. Phys.* **1995**, *102*, 5118. (b) Ludwig, R.; Bohmann, J.; Farrar, T. C. *J. Phys. Chem.* **1995**, *99*, 9681.

(4) (a) Beesley, A. H.; Evans, D. F.; Laughlin, R. G. *J. Phys. Chem.* **1988**, *92*, 791. (b) Auvray, X.; Petipas, C.; Anthore, R.; Rico, I.; Lattes, A. *Ibid.* **1989**, *93*, 7458 and references therein.

(5) Mohandas, P.; Singh, S. *J. Mol. Struct. (THEOCHEM)* **1990**, *361*, 229 and references therein.

(6) (a) Kirchhoff, W. H.; Johnson, D. R. *J. Mol. Spectrosc.* **1973**, *45*, 159. (b) Hirota, E.; Sugisaki, R.; Nielsen, C. J.; Sørensen, G. O. *Ibid.* **1974**, *49*, 251. (c) Florián, J.; Johnson, B. G. *J. Phys. Chem.* **1994**, *98*, 3681 and references therein.

(7) (a) Kurland, R. J.; Wilson, E. B., Jr. *J. Chem. Phys.* **1957**, *27*, 585. (b) Kukolich, S. G.; Nelson, A. C. *Chem. Phys. Lett.* **1971**, *11*, 383.

(8) (a) Sunners, B.; Piette, L. H.; Schneider, W. G. *Can. J. Chem.* **1960**, *38*, 681. (b) Hinton, J. F.; Ladner, K. K.; Stewart, W. E. *J. Magn. Reson.* **1973**, *12*, 90. (c) Barboiu, V.; Petrescu, V. *Org. Magn. Reson.* **1973**, *5*, 43. (d) Dorman, D. E.; Bovey, F. A. *J. Org. Chem.* **1973**, *38*, 1719. (e) Sørensen, O. W.; Scheibye, S.; Lawesson, S.-O.; Jakobsen, H.-J. *Org. Magn. Reson.* **1981**, *16*, 322. (f) Burgar, M. I.; St. Amour, T. E.; Fiat, D. *J. Phys. Chem.* **1981**, *85*, 502.

(9) Chuck, R. J.; Gillies, D. G.; Randall, E. W. *Mol. Phys.* **1969**, *16*, 121.

(10) Reeves, L. W.; Riveros, J. M., Spragg, R. A.; Vanin, J. A. *Mol. Phys.* **1973**, *25*, 9.

(11) Sykora, S.; Vogt, J.; Bösiger, H.; Diehl, P. *J. Magn. Reson.* **1979**, *36*, 53.

(12) (a) Lounila, J.; Diehl, P. *J. Magn. Reson.* **1984**, *56*, 254. (b) Lounila, J. *Mol. Phys.* **1986**, *58*, 897.

(13) *CRC Handbook of Chemistry and Physics*, 48th ed.; Chemical Rubber Co.: Cleveland, OH, 1967.

(14) Ribas Prado, F.; Giessner-Prettre, C. *J. Magn. Reson.* **1982**, *47*, 103.

(15) Barszczewicz, A.; Jaszuński, M.; Jackowski, K. *Chem. Phys. Lett.* **1993**, *203*, 404.

(16) Jackowski, K.; Jaszuński, M.; Makulski, W. *J. Magn. Reson.*, in press.

(17) Kirby, C. W.; Lumsden, M. D.; Wasylishen, R. E. *Can. J. Chem.* **1995**, *73*, 604.

(18) Palmer, M. H.; Sherwood, P. *Z. Naturforsch.* **1996**, *51A*, 460.

(19) Eichele, K.; Lumsden, M. D.; Wasylishen, R. E. *J. Phys. Chem.* **1993**, *97*, 8909.

(20) Lumsden, M. D.; Wasylishen, R. E.; Eichele, K.; Schindler, M.; Penner, G. H.; Power, W. P.; Curtis, R. D. *J. Am. Chem. Soc.* **1994**, *116*, 1403.

(21) (a) Gerald, R., II; Bernhard, T.; Haeberlen, U.; Rendell, J.; Opella, S. *J. Am. Chem. Soc.* **1993**, *115*, 777. (b) Usha, M. G.; Peticolas, W. L.; Wittebort, R. J. *Biochemistry* **1991**, *30*, 3955.

(22) Ylihautala, M.; Vaara, J.; Ingman, P.; Jokisaari, J.; Diehl, P. *J. Phys. Chem. B* **1997**, *101*, 32.

(23) Møller, Chr.; Plesset, M. S. *Phys. Rev.* **1934**, *46*, 1.

(24) Bartlett, R. J.; Purvis, G. D. *Int. J. Quantum Chem. 14*, **1978**, 561. Pople, J. A.; Krishnan, R.; Schlegel, H. B.; Binkley, J. S. *Ibid.* **1978**, *14*, 545.

(25) Pople, J. A.; Head-Gordon, M.; Raghavachari, K. *J. Chem. Phys.* **1987**, *87*, 5968.

(26) Parr, R. G.; Yang, W. *Density-Functional Theory of Atoms and Molecules*; Oxford University Press: New York, 1989.

(27) Vahtras, O.; Ågren, H.; Jørgensen, P.; Jensen, H. J. Aa.; Padkjær, S. B.; Helgaker, T. *J. Chem. Phys.* **1992**, *96*, 6120.

(28) Jackowski, K. *Chem. Phys. Lett.* **1992**, *194*, 167.

(29) *Nuclear Magnetic Resonance of Liquid Crystals*; Emsley, J. W., Ed.; D. Reidel Publishing: Dordrecht, 1985.

(30) Lounila, J.; Wasser, R.; Diehl, P. *Mol. Phys.* **1987**, *62*, 19.

(31) Kaski, J.; Vaara, J.; Jokisaari, J. *J. Am. Chem. Soc.* **1996**, *118*, 8879.

(32) Kaski, J.; Lantto, P.; Vaara, J.; Jokisaari, J. Manuscript in preparation.

(33) Lounila, J.; Jokisaari, J. *Prog. Nucl. Magn. Reson. Spectrosc.* **1982**, *15*, 249.

(34) Helgaker, T.; Jensen, H. J. Aa.; Jørgensen, P.; Koch, H.; Olsen, J.; Ågren, H.; Bak, K. L.; Bakken, V.; Christiansen, O.; Halkier, A.; Dahle, P.; Heiberg, H.; Hettema, H.; Jonsson, D.; Kobayashi, R.; de Meras, A. S.; Mikkelsen, K. V.; Normann, P.; Ruud, K.; Taylor, P. R.; Vahtras, O. DALTON, an electronic structure program, 1996.

(35) Frisch, M. J.; Trucks, G. W.; Schlegel, H. B.; Gill, P. M. W.; Johnson, B. G.; Robb, M. A.; Cheeseman, J. R.; Keith, T.; Petersson, G. A.; Montgomery, J. A.; Raghavachari, K.; Al-Laham, M. A.; Zakrzewski, V. G.; Ortiz, J. V.; Foresman, J. B.; Cioslowski, J.; Stefanov, B. B.; Nanayakkara, A.; Challacombe, M.; Peng, C. Y.; Ayala, P. Y.; Chen, W.; Wong, M. W.; Andres, J. L.; Replogle, E. S.; Gomperts, R.; Martin, R. L.; Fox, D. J.; Binkley, J. S.; Defrees, D. J.; Baker, J.; Stewart, J. P.; Head-Gordon, M.; Gonzalez, C.; Pople, J. A. *Gaussian 94, Revision B.1*; Gaussian, Inc.: Pittsburgh, PA, 1995.

(36) (a) London, F. *J. Phys. Radium* **1937**, *8*, 397. (b) Ditchfield, R. *J. Chem. Phys.* **1972**, *56*, 5688. (c) Wolinski, K.; Hinton, J. F.; Pulay, P. *J. Am. Chem. Soc.* **1990**, *112*, 8251.
(37) Helgaker, T.; Jørgensen, P. *J. Chem. Phys.* **1991**, *95*, 2595.
(38) Ruud, K.; Helgaker, T.; Kobayashi, R.; Jørgensen, P.; Bak, K. L.; Jensen, H. J. Aa. *J. Chem. Phys.* **1994**, *100*, 8178.
(39) Stevens, R. M.; Pitzer, R. M.; Lipscomb, W. N. *J. Chem. Phys.* **1963**, *38*, 550.
(40) Gauss, J. *J. Chem. Phys.* **1993**, *99*, 3629.
(41) Cheeseman, J. R.; Trucks, G. W.; Keith, T. A.; Frisch, M. J. *J. Chem. Phys.* **1996**, *104*, 5497.
(42) *Nuclear Magnetic Shieldings and Molecular Structure*; Tossel, J. A., Ed.; Kluwer: Dordrecht, 1993.
(43) Snyder, L. C. *J. Chem. Phys.* **1978**, *68*, 291.
(44) Gerber, S.; Huber, H. *J. Mol. Spectrosc.* **1989**, *134*, 168; *Chem. Phys.* **1989**, *134*, 279.
(45) Vaara, J.; Hiltunen, Y. *J. Chem. Phys.*, in press.
(46) Ludwig, R.; Weinhold, F.; Farrar, T. C. *J. Chem. Phys.* **1996**, *105*, 8223.
(47) (a) Pyykkö, P.; Li, J. *Report HUKI 1-92*; Department of Chemistry, University of Helsinki: Helsinki, 1992. (b) Tokman, M.; Sundholm, D.; Pyykkö, P.; Olsen, J. *Chem. Phys. Lett.* **1997**, *265*, 60.
(48) (a) Jørgensen, P.; Jensen, H. J. Aa.; Olsen, J. *J. Chem. Phys.* **1988**, *89*, 3654. (b) Olsen, J.; Yeager, D. L.; Jørgensen, P. *Ibid.* **1989**, *91*, 381.
(49) Contreras, R. H.; Facelli, J. C. *Annu. Rep. Nucl. Magn. Reson. Spectrosc.* **1993**, *27*, 255.
(50) Suhai, S. *J. Chem. Phys.* **1995**, *103*, 7030.
(51) DeSando, R. J.; Brown, G. H. *J. Phys. Chem.* **1968**, *72*, 1088.
(52) Roos, B. O. In *Lecture Notes in Quantum Chemistry*; Roos, B. O., Ed.; Springer-Verlag: Berlin, 1992.
(53) Vosko, S. H.; Wilk, L.; Nusair, M. *Can. J. Phys.* **1980**, *58*, 1200.
(54) Becke, A. D. *Phys. Rev. A* **1988**, *38*, 3098.
(55) Lee, C.; Yang W.; Parr, R. G. *Phys. Rev. B* **1988**, *37*, 785.
(56) Perdew, J. P.; Wang, Y. *Phys. Rev. B* **1992**, *45*, 13244. Perdew, J. P.; Chevary, J. A.; Vosko, S. H.; Jackson, K. A.; Pederson, M. R.; Singh, D. J.; Fiolhais, C. *Phys. Rev. B* **1992**, *46*, 6671.
(57) Schindler, M.; Kutzelnigg, W. *J. Chem. Phys.* **1982**, *76*, 1919.
(58) Barszczewicz, A.; Helgaker, T.; Jaszuński, M.; Jørgensen, P.; Ruud, K. *J. Chem. Phys.* **1994**, *101*, 6822; *J. Magn. Reson. A* **1995**, *114*, 212.
(59) Jaszuński, M.; Szymanski, S.; Christiansen, O.; Jørgensen, P.; Helgaker, T.; Ruud, K. *Chem. Phys. Lett.* **1995**, *243*, 144.
(60) Huzinaga, S. *Approximate Atomic Functions*; University of Alberta: Edmonton, 1971.
(61) Laatikainen, R.; Niemitz, M.; Weber, U.; Sundelin, J.; Hassinen, T.; Vepsäläinen, J. *J. Magn. Reson. A* **1996**, *120*, 1.
(62) Bock, C. W.; Trachtman, M. *J. Mol. Spectrosc.* **1981**, *89*, 76.
(63) Wasser, R.; Kellerhals, M.; Diehl, P. *Magn. Reson. Chem.* **1989**, *27*, 335.
(64) Jameson, A. K.; Jameson, C. J. *Chem. Phys. Lett.* **1987**, *134*, 461.
(65) Jameson, C. J.; de Dios, A. C.; Jameson, A. K. *J. Chem. Phys.* **1991**, *95*, 1069.
(66) Wasylishen, R. E.; Mooibroek, S.; MacDonald, J. B. *J. Chem. Phys.* **1984**, *81*, 1057.
(67) The improved strategy in choosing the active spaces was kindly suggested by Prof. Trygve Helgaker.
(68) Rauhut, G.; Puyear, S.; Wolinski, K.; Pulay, P. *J. Phys. Chem.* **1996**, *100*, 6310.
(69) Olsson, L.; Cremer, D. *J. Chem. Phys.* **1996**, *105*, 8995.
(70) Lee, A. M.; Handy, N. C.; Colwell, S. M. *J. Chem. Phys.* **1995**, *103*, 10095.
(71) Kálmán, E.; Serke, I.; Pálinkás, G.; Zeidler, M. D.; Wiesmann, F. J.; Bertagnolli, H.; Chieux, P. *Z. Naturforsch.* **1983**, *38A*, 231.
(72) (a) Chesnut, D. B.; Phung, C. G. In *Nuclear Magnetic Shieldings and Molecular Structure*; Tossell, J. A., Ed.; Kluwer: Dordrecht, 1993. (b) Chesnut, D. B.; Phung, C. G. *Chem. Phys. Lett.* **1991**, *183*, 505. (c) de Dios, A. C.; Oldfield, E. *J. Am. Chem. Soc.* **1994**, *116*, 11485.
(73) Asakura, T.; Niizawa, Y.; Williamson, M. P. *J. Magn. Reson.* **1992**, *98*, 646. Stark, R. E.; Jelinski, L. W.; Ruben, D. J.; Torchia, D. A.; Griffin, R. G. *Ibid.* **1983**, *55*, 266.
(74) Asakawa, N.; Kuroki, S.; Kurosu, H.; Ando, I.; Shoji, A.; Ozaki, T. *J. Am. Chem. Soc.* **1992**, *114*, 3261.
(75) Michal, C. A.; Wehman, J. C.; Jelinski, L. W. *J. Magn. Reson. B* **1996**, *111*, 31. Prosser, R. S.; Daleman, S. I.; Davis, J. H. *Biophys. J.* **1994**, *66*, 1415.